Chemical Engineering Journal 108 (2005) 35–45

Chemical Engineering Journal

www.elsevier.com/locate/cej

Regime transition in a gas–liquid–solid fluidized bed

Maytinee Vatanakul[a], Ying Zheng[a,*], Lufei Jia[b], Kai Zhang[a]

[a] *Department of Chemical Engineering, University of New Brunswick, 15 Dineen Drive, P.O. Box 4400, Fredericton, N.B., Canada E3B 5A3*
[b] *CANMET Energy Technology Center, 1 Haanel Drive, Ottawa, ON, Canada K1A 1M1*

Received 13 December 2003; received in revised form 22 August 2004; accepted 14 December 2004

Abstract

A mathematical approach, based on the discriminant analysis of the fluctuations of the voltage signals, is proposed for the first time to identify the boundary between the particulate and the circulating three-phase fluidization regimes. In this new method, the particle size, liquid viscosity, gas flow rate, superficial liquid velocity, and solid circulating rate, which significantly affect on the characteristics of the voltage signals, are selected as the discriminant variables. The new approach proved to be a reliable method to determine the transition velocity between the particulate and the circulating fluidization regimes. The effects of particle size, liquid viscosity, and gas flow rate on the transition velocity are investigated as well.

Keywords: Three-phase fluidized bed; Transition; Discriminant analysis; Flow characteristics

1. Introduction

Gas–liquid–solid three-phase fluidized bed is one of the most important multiphase reactors for physical, chemical, and biochemical processes. In a three-phase fluidized bed, upward liquid and gas phases induce the fluidization of the solid particles. The flow structure is a combination of the gas–liquid bubbly flow and the liquid–solid vertical upflow. With increasing liquid and gas velocities, the fluidized bed can be categorized by the state of solid motion into four different regimes: the packed bed regime, the particulate liquid fluidization regime, the circulating fluidization regime and the dilute liquid transport regime [1,2].

As a fluid flows upward through an assemblage of solid particles, the minimum fluidization condition is reached when the upward drag force acting on the individual solid particle balances with the force of gravity and the buoyant force or, in other words, when the pressure drop across the bed equals the weight of the bed per unit area. Below this minimum fluidization, the bed is in the packed or fixed bed regime. At the transition of fluidization, the flow system actually corresponds to the loosest state of a packed bed of hardly any weight and the packed bed starts to expand [3,4]. Above this minimum fluidization condition, the bed experiences the expanded bed or conventional fluidization regime. In this regime, the solid bed continuously expands to accommodate the increased flow. The particles move apart from each other, and small vibrations take place. The bed of three-phase flow can be divided into two regions, which are the main fluidized bed region with a high concentration of solid particles and the freeboard region with no solid particles present. In the main fluidized bed region or the dense bed region, the solid holdup is uniformly distributed across the bed. There is a minimum axial transport property variation in this region. Gas and liquid velocities have no influence on the solid profile [5–9].

With further increase in the liquid and/or gas velocities, the surface of the bed disappears and solid particles start to be entrained out of the bed with the fluid stream [1,3]. The continuous solids feeding to the bottom of the bed is essential for the fluidization system to enter the three-phase circulating regime. The main characteristics of a circulating fluidized bed are the continuous solid feeding and carry-over of solid particles between the riser and the downer. The boundary of this carry-over behavior can be identified by the transition of

* Corresponding author. Tel.: +1 506 447 3329; fax: +1 506 453 3591.
E-mail address: yzheng@unb.ca (Y. Zheng).

1385-8947/$ – see front matter © 2004 Elsevier B.V. All rights reserved.
doi:10.1016/j.cej.2004.12.035

Nomenclature

b	sum of squared differences between groups for each variable
c	discriminant coefficient
d_p	particle diameter (m)
d_o	difference between the means of the two groups for the discriminant variables
D^2	Mahalanobis's distance
G_s	particle circulating rate (kg/m^2 s)
H_0	null hypothesis
m	number of cases
Q	flow rate (mL/s)
s	matrix of pooled variances referring to the discriminant variables
U	velocity (m/s)
w	within-group sum of squared differences
X_j	discriminant variable
X_{jkm}	distinguished characteristics X_j in the group k for the case m
$\bar{X}$	mean of the discriminant variable
Y_{km}	value of the discriminant function of the group k for the case m

Greek letters

ε	phase holdup
μ	viscosity (cP)
ρ	density (kg/m^3)

Subscripts

g	gas phase
k	group number
l	liquid phase
m	case number
s	solid phase

circulating operation, for which the liquid velocity is equal to the critical transition velocity, U_{lc}. This transition velocity is defined as the velocity at which the particle circulation rate changes from zero to a non-zero value [2]. Within this circulating fluidization regime, the pressure between the riser and the downer is well balanced. This pressure balance between the two columns controls the circulating condition and influences the lower boundary of the circulating fluidization [10]. Solid particles circulate in the fluidization unit, and gas bubbles are small and distributed uniformly along the bed. As the liquid velocity keeps increasing, the pressure gradient decreases. Finally, the transition of the transport fluidization regime is marked at the critical liquid velocity, U_{lt}, which is the upper limit velocity for the circulating fluidization regime. At this state, the pressure gradients at every elevation in the riser column are finally equal, which implies uniform distribution of solid particles along the riser [2,10]. This critical velocity can also be determined as the minimum velocity for maintaining the operating stability of the riser at a constant solid circulation rate.

In order to study the fluidization's hydrodynamic behaviors, it is important to predict the transition velocities at the boundary between different fluidization regimes. There are a number of experimental data and numerical correlations available for the boundary between the packed bed and expanded bed regimes [11–13]. However, knowledge of the transition between the expanded and the circulating fluidization regimes as well as the transition between the circulating fluidization and the liquid transport regimes in a three-phase fluidized bed is still limited.

In this work, the behaviors of voltage signals were investigated under a wide range of operating conditions in a three-phase reactor. Three different methods—the new approach based on the discriminant analysis of the conductivity voltage signals, the measurement of pressure profile, and the measurement of solid circulating rate—were used to define the boundary between the particulate and circulating fluidization regimes as well as the transition velocity of circulating fluidization and transport fluidization. The influences of particle size, liquid viscosity, and gas flow rate on the transition velocity were studied as well.

2. Experimental set-up

Fig. 1 shows the set-up of a gas–liquid–solid three-phase circulating fluidized bed, GLSCFB, consisting of two main Plexiglas columns. The vertical Plexiglas riser column is 7.6 cm in diameter and 2.0 m in height, and the vertical Plexiglas downer column is 10 cm in diameter. Glass beads with average diameters of 433 μm, 700 μm and 1300 μm and a density of 2500 kg/m^3, were used as the solid phase. Oil-free air was used as the gas phase. Tap water and sugar–water mixtures, having viscosities of 1.8 and 3.5 cP were used as the liquid phase. The liquid pumped from the reservoir is divided into two streams with the primary liquid stream entering the bottom of the riser and carring particles up to the top of the riser where they are separated by a vortex-filter. The auxiliary liquid stream enters at the side of the downer and controls the amount of particles sent into the riser via the L-valve. The superficial liquid velocity is the sum of the primary and auxiliary liquid flow rates. If the auxiliary liquid flow rate is set to zero, there is no solid particle flowing to the riser, and the solid circulation cannot be achieved in the CFB unit even though a high primary liquid flow rate is applied. With increasing auxiliary liquid flow rate more solid particles are circulated in the riser so that the solid circulation rate increases. The solid circulating rate is determined by measuring particle mass, which are collected in a section above the butterfly valve, for a given time period. The solid circulating rate and liquid velocity in the riser can be controlled independently by regulating the flow ratio between the two liquid streams. A gas distributor, a perforated stainless steel plate

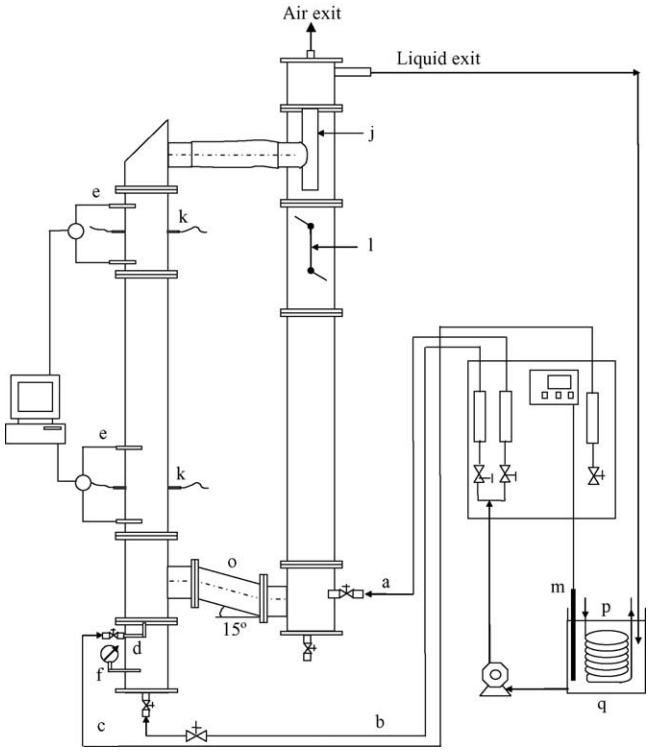

Fig. 1. The model gas–liquid–solid circulating fluidized bed column: (a) auxiliary liquid line, (b) main liquid line, (c) air line, (d) gas distributor, (e) pressure transducers, (f) pressure control valve, (g) heat controller, (h) riser, (i) downer, (j) vortex-filter, (k) conductivity probes, (l) butterfly valve, (m) heater, (n) flow meters, (o) L-valve, (p) cooling coil, (q) water reservoir, (r) personal computer.

with small pores of 35 μm diameter located at the riser base, is used to create fairly uniform gas bubbles. All experiments were carried out at ambient temperature.

Pressure transducers and wall electrical conductivity probes were used to measure the pressure gradients and the voltages at two axial positions, 0.5 and 1.45 m from the gas distributor. A pair of electrodes was simultaneously supplied with a 1 kHz ac current. The pressure transducers and wall conductivity probes were connected to a data acquisition system, which measured the data at frequency of 150 Hz for 30 s. The software "Visual Designer" was employed to record the data of pressure drop and conductivity simultaneously.

As mentioned earlier, three different measurement techniques were applied to determine the transition velocities within a three-phase fluidized bed. For the experimental setup of the pressure profile and the solid circulating rate methods, the particles were first packed in the riser column. Then the auxiliary flow was set at a constant value of 1.38 cm/s, for all the experiments. For each set of experiments, a constant gas flow rate was used. Four different gas flow rates, 0, 35.1, 66.6 and 113.6 mL/s, were introduced in the fluidization unit. The primary liquid flow was increased gradually until the transport regime of solid particles was reached. After each increment of the primary liquid velocity, once the system was stable, the pressure gradients, the solid circulating rate, and the electrical conductivity signals were measured at the same time.

3. Discriminant analysis

The discriminant analysis uses continuous measurements on different groups of items to highlight aspects that distinguish the groups and to use these measurements to classify new items. The discriminant function is a linear combination of variables and can be defined as follows [14]:

$$Y_{km} = c_1 X_{1km} + c_2 X_{2km} + \cdots + c_n X_{nkm} \quad (1)$$

The discriminating variable, X_{ikm}, is the distinguished characteristics X_i in the group k for the case m. Y_{km} is the value of the discriminant function of the group k for the case m. c is the coefficient, which produces the desired characteristics in the function.

For example, a system has two groups, A and B, which also can be commonly called clusters. These groups are both relatively homogeneous. The items of each group clearly differ in their behavior with respect to the variables. To summarize the position of a group, imaginary points, Y_A and Y_B, representing centroids, which coordinate the groups' means, can be calculated.

$$Y_A = \sum_{i=1}^{l} c_i \bar{X}_{iA}, \qquad Y_B = \sum_{i=1}^{l} c_i \bar{X}_{iB}, \quad i = 1, \ldots, l \quad (2)$$

and $\bar{X}_{ok}$ is the mean of the variable X_{oki} ($i = 1, \ldots, m_k$).

$$\bar{X}_{oA} = \frac{1}{m_A} \sum_{i=1}^{m_A} X_{oAi} \quad \text{and} \quad \bar{X}_{oB} = \frac{1}{m_B} \sum_{i=1}^{m_B} X_{oBi} \quad (3)$$

where m_A and m_B are the number of cases in groups A and B.

The first step of the analysis is to find the coefficients c_i ($i = 1, \ldots, n$). For this purpose, two n-dimensional matrices b and w are defined. The diagonal of b is the sum of squared differences between groups for each variable and the diagonal element of w is the within-group sum of squared differences.

$$w_{ij} = \sum_{k=1}^{2} \sum_{m=1}^{m_k} (X_{ikm} - \bar{X}_{ik})(X_{jkm} - \bar{X}_{jk})$$

and

$$b_{ij} = \sum_{k=1}^{2} \sum_{m=1}^{m_k} (X_{ikm} - \bar{X}_i)(X_{jkm} - \bar{X}_j) - \sum_{k=1}^{2} \sum_{m=1}^{m_k} (X_{ikm} - \bar{X}_{ik})(X_{jkm} - \bar{X}_{jk}) \quad (4)$$

where m_k is the number of the cases in the group k, $\bar{X}_i$ is the total mean value of the variable X_i for all cases.

The value of the discriminant function differentiates group-means in such a way that minimizes the within-group difference (w) and simultaneously maximizes the between-group difference (b). This can be implemented by solving a maximization problem.

$$\text{Max}\left[\frac{c'bc}{c'wc}\right] \tag{5}$$

expressed in terms of differential calculus as

$$\frac{\partial}{\partial c}\left[\frac{c'bc}{c'wc}\right] = 0 \tag{6}$$

In this study, two groups, A and B are considered. The data in each group are classified into two variables X_1 and X_2. Therefore, through the uses of calculus and other mathematical operations, the system presented in Eq. (6) can be simplified as follows [15]:

$$\lfloor s_{ij} \rfloor \lfloor c_j \rfloor = \lfloor d_j \rfloor \tag{7}$$

with [16],

$$s_{\text{oq}} = \sum_{i=1}^{m_\text{A}} \{(X_{\text{oA}i} - \bar{X}_{\text{oA}})(X_{\text{qA}i} - \bar{X}_{\text{qA}})\} + \sum_{i=1}^{m_\text{B}} \{(X_{\text{oB}i} - \bar{X}_{\text{oB}})(X_{\text{qB}i} - \bar{X}_{\text{qB}})\} \tag{8}$$

where the s is the matrix of pooled variances referring to two variables and the d_o is the difference between the means of the two groups for variables X_1 and X_2, which is given by

$$d_\text{o} = \bar{X}_{\text{oA}} - \bar{X}_{\text{oB}} \tag{9}$$

The c_j coefficient can then be calculated using Eq. (7). The function of linear combination of these variables can be solved. From this linear function, all the terms can be added together to yield a single number, which is called the discriminant index, Y_AB. This number is the point along the discriminant function line that is exactly the mid-point between the centroids of groups A and B.

$$Y_\text{AB} = \frac{m_\text{A} Y_\text{A} + m_\text{B} Y_\text{B}}{m_\text{A} + m_\text{B}} \tag{10}$$

The discriminant index can be used to allocate new samples of unknown origin to one of these two original groups.

The significance of the separation between the two groups used in the discriminant function needs to be tested. To do so, the distance, called Mahalanobis's distance or the generalized distance, denoted as D^2, is calculated. This distance is equivalent to the differences between the two multivariate means,

$$D^2 = (m_\text{A} + m_\text{B} - p)\{c_1(\bar{X}_{1\text{A}} - \bar{X}_{1\text{B}}) + c_2(\bar{X}_{2\text{A}} - \bar{X}_{2\text{B}})\} \tag{11}$$

The F-test of this distance has the form [15],

$$F = \left(\frac{m_\text{A} + m_\text{B} - p - 1}{(m_\text{A} + m_\text{B} - 2)p}\right)\left(\frac{m_\text{A} m_\text{B}}{m_\text{A} + m_\text{B}}\right) D^2 \tag{12}$$

with p and $(m_\text{A} + m_\text{B} - p - 1)$ degree of freedom. p is the number of variables. The null hypothesis tested by this criterion is that the two multivariate means are equal, or that the distance between them is zero. That is,

$$H_0 : [d_\text{o}] = 0$$

against

$$H_1 : [d_\text{o}] > 0$$

The appropriateness of this equation as a test of a discriminant function should be apparent. If the means of the two groups are very close together, it will be hard to separate them. In contrast, if the two means are well separated and the data of each group are scattered about the means, the boundary of the discrimination will be clear.

This is a new attempt to apply the discriminant analysis to define the boundary between the particulate regime (group A) and circulating regime (group B) of a three-phase fluidization system. The experimental data obtained from the conductivity probes in the known regimes were used to find the discriminant function. In this work, two different approaches based on this discriminant analysis were performed.

4. Results and discussion

4.1. Fluctuations of conductivity signals

The voltage signals recorded through the conductivity probes in the three-phase fluidized bed under a wide range of operating conditions are presented here. The conductivity signals are stable in pure liquid phase. The slight fluctuations of the conductivity signals are considered as the noise created by the conductivity tester and have been subtracted from all experimental data.

Fig. 2 shows the signals recorded from the 3ph-FB and GLSCFB using 1300 μm glass beads. It can be seen clearly that the signal of the voltage difference in the GLSCFB fluctuated less than that in 3ph-FB. The shape and high peaks represent the presence of gas bubbles. In the three-phase circulating flow, the system operated at a higher total liquid velocity. At high liquid velocity, relatively large bubbles were broken up by the intensified shear stress. In addition, the bubbles flowed upward faster, reducing, in turn, their chance to coalesce. Thus, gas bubbles distributed more uniformly in the riser column. This characteristic led to fewer fluctuations in the signals [17,18].

The voltage signals in the three-phase system present an interesting outcome. The experimental results obtained in this work clearly show that the fluctuations of voltages are affected by many operating conditions. The influence of the

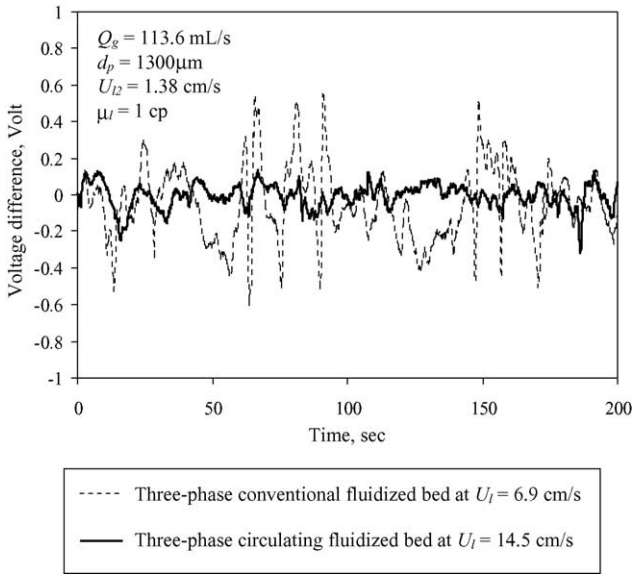

Fig. 2. The relationship between Y and liquid velocity for the comprehensive study of the discriminant analysis.

total liquid velocity on the standard deviation of the voltage signals is shown in Fig. 3a, for the systems of pure water under various gas flow rates. Four hundred and thirty-three micrometer glass beads were used for the solid phase. The curve of voltage fluctuations can be clearly separated into two zones. The first portion of the curve at relatively low liquid velocity has a sharp decrease in standard deviation with increasing liquid velocity, representing the particulate fluidization regime. In the second portion of the curve, the decrease of standard deviation becomes graduated with increasing liquid velocity. This section was the characteristics of circulating fluidization regime. In a fluidization system, the higher liquid velocity resulted in smaller gas bubbles, leading to less fluctuation in the signals. In addition, similar trends were also observed for the systems of 700 and 1300 μm glass beads with a constant gas flow rate of 35.1 mL/s as shown in Fig. 3b. In the system of the bigger glass beads, the transition between the two zones took place at a higher liquid velocity due to a higher terminal velocity of solid particles. It is also seen that the standard deviation increased when the particle size increased at the same liquid velocity. But the influence of bead size was less dominant at a high liquid velocity. The sharp decrease in the standard deviation of the voltage signal was clearly observed in the system of 1300 μm glass beads. An increase in the liquid velocity induced enough drag force on the solid particles to overcome the interaction force between phases. The particles were dragged upward and the fluctuations of the signals were consequently decreased. Therefore, the liquid velocity was clearly the dominant factor for the standard deviation of the electrical voltages.

The gas flow rate was another important factor influencing the voltage fluctuation presented in Fig. 3a for the system of pure water, and Fig. 4a and b for the system of 1.8-cP and 3.5-cP sugar–water mixtures, respectively. The standard deviation of the voltage signals increased when the gas flow rate increased for every liquid system. A higher gas flow rate generated more wakes in the riser. They enhanced interactions between phases and resulted in more fluctuations of the voltage signals.

The effect of liquid viscosity on the fluctuation of the voltage signals is presented in Fig. 5. The 1.8-cP, 3.5-cP sugar–water mixtures and 1 cP-pure water were used as continuous liquid phases. The experiments were conducted at a fixed gas flow rate of 35.1 mL/s and four different liquid velocities. The standard deviations of voltage were gradually reduced with increasing liquid viscosity. This characteristic can be explained by a higher liquid viscosity creating a higher

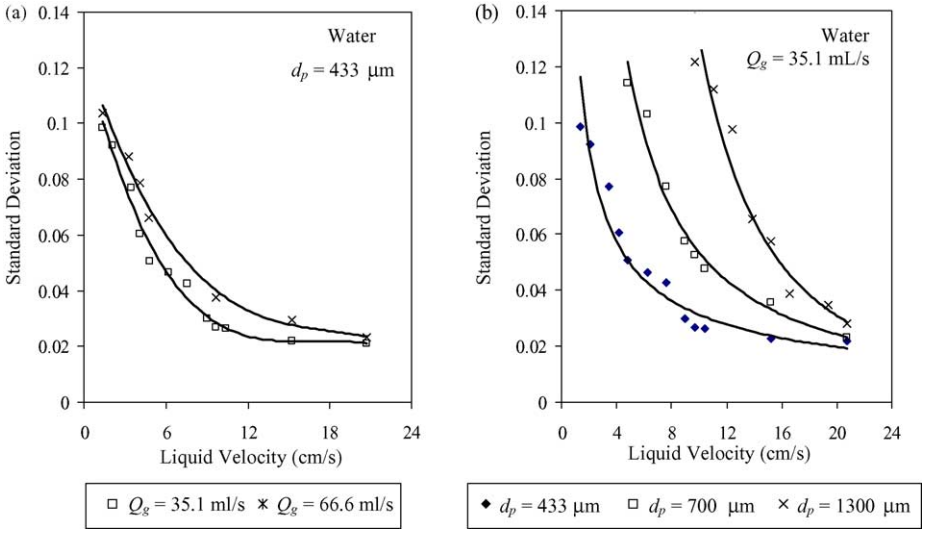

Fig. 3. The effect of the liquid velocity on the standard deviaiton of voltage signal for (a) under various gas flow rates, (b) for three different particle systems with fixed gas flow rate of 35.1 mL/s.

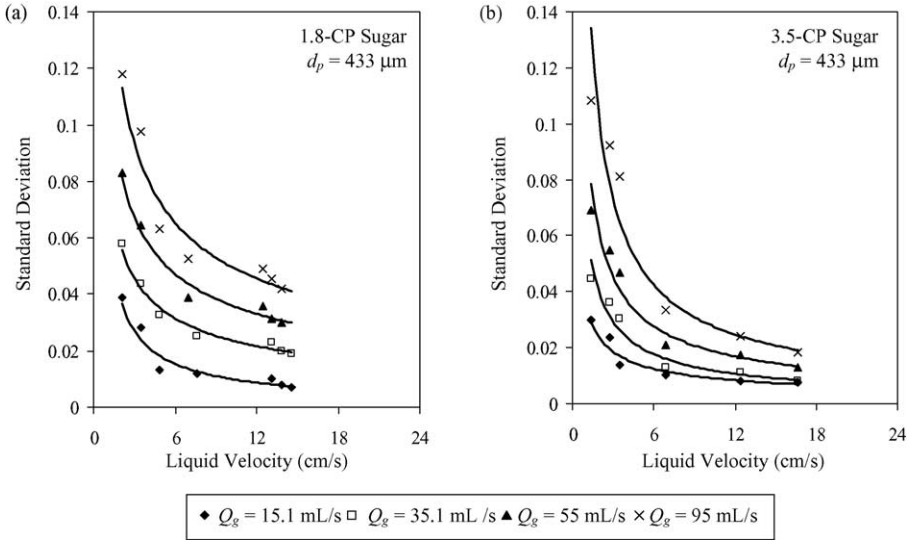

Fig. 4. The effect of the liquid velocity on the standard deviation of voltage signal under various gas flow rates for (a) 1.8-cP sugar–water mixture system, (b) 3.5-cP sugar–water mixture system.

drag force on the particle surface and forcing the dispersed phases to move in one direction. This phenomenon led to small interactions between phases. In addition, the results also indicated that liquid velocity reduced the effect of liquid viscosity on the voltage signal fluctuations.

The signals of the conductivity voltage provided interesting results that could be used to identify the transition boundary of a three-phase fluidization system.

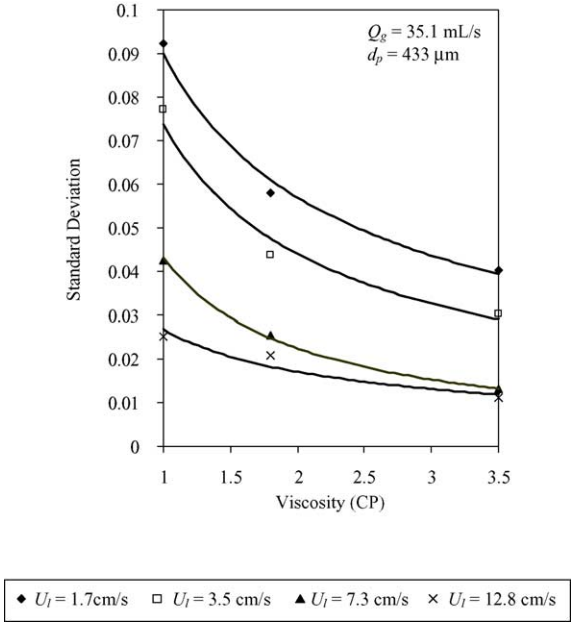

Fig. 5. The fluctuation of the voltage difference measured in the three-phase expanded and circulating fluidized bed for 433-μm glass beads under fixed liquid viscosity, gas flow rate and auxiliary velocity of 1 cP, 113.6 mL/s and 1.38 cm/s, respectively.

4.2. The boundary between the expanded and the circulating three-phase flows

4.2.1. Discriminant approach

From the observation presented in the previous section, the fluctuations of conductivity signals showed distinct features in the expanded bed and in the circulating fluidization regime. The liquid velocity appeared to be a dominant factor for the transition boundary between the two fluidization regimes. Therefore, the liquid velocity and standard deviation of conductivity signals were used as the variables of discriminant analysis. The discriminant analysis was then applied to each set of the experimental data of known regime. These data were separated into two groups A and B: expanded and circulating fluidization regimes and the values of Y_A and Y_B are determined using the method described in Section 3. The discriminant index, Y_{AB}, was computed using Eq. (10). The computed Y_A and Y_B can be plotted in the same graph as a function of liquid velocity. Fig. 6 shows an example of Y_A and Y_B versus liquid velocity when the fluidized bed is operated at a gas flow rate of 66.6 mL/s. The transition liquid velocity can be obtained when the fitting equation was set to be equal to the discriminant index value, which was 13.6 cm/s as indicated on the curve of Fig. 6.

The same analysis was applied for all other experimental results. The transition velocity can then be expressed as a function of the operating conditions, liquid property, and particle size. The effect of particle sizes on the transition liquid velocity is shown in Fig. 7. It can be seen that bigger particles lead to a higher transition liquid velocity from the expanded bed to the circulating fluidization regime. Fig. 7 also shows the influence of the gas flow rate on the transition velocity. In the system of 433-μm glass beads, the transition velocity clearly decreased with increasing gas flow rate. This

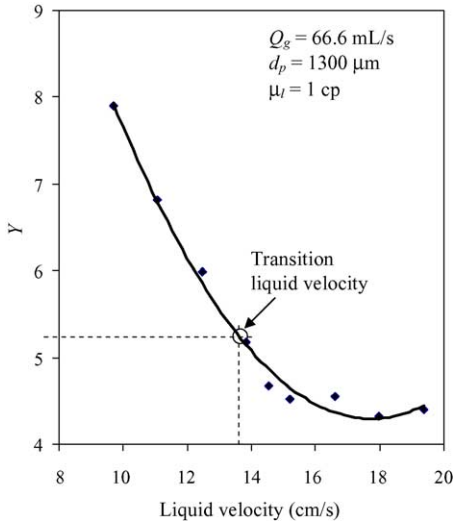

Fig. 6. The relationship between Y and liquid velocity of the discriminant analysis based on the liquid velocity effect under the operating conditions of 66.6 mL/s gas flow rate, 1 cP water and 1300 μm glass beads.

observation was also obtained in the work of Liang et al. [2] The same effect of gas flow rate on the transition liquid velocity can also be observed in the 433-μm bead system of higher liquid viscosity (3.5 cP) as shown in Fig. 8.

On the other hand, in Fig. 7, gas flow rate presented interesting impact on the two bigger particle systems (700-μm

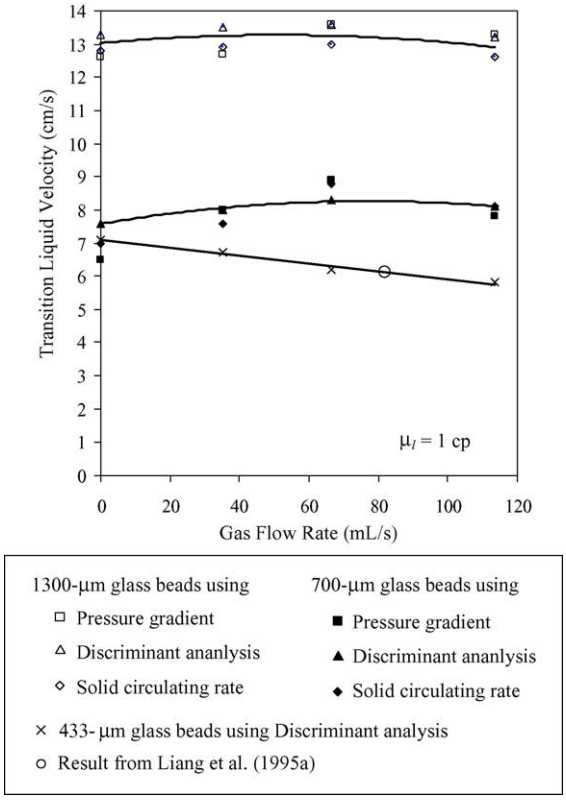

Fig. 7. The effect of gas flow rate on the transition liquid velcoity of the circualting fluidizaiton regime measured by three different mehtods for systems of three different particle sizes.

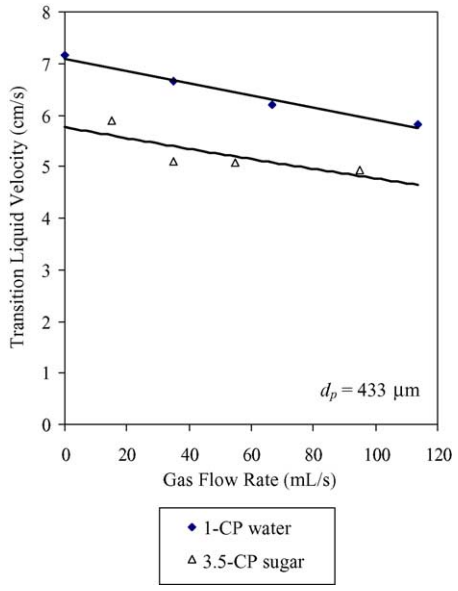

Fig. 8. The effect of gas flow rate on the transition liquid velcoity of the circualting fluidizaiton regime for two different liquid viscosity systems of 433-μm glass beads.

and 1300-μm glass beads). The transition velocity first increased when the gas flow rate increased. Beyond a gas flow rate at approximate 66 mL/s, the transition liquid velocity slightly decreased with further increase in the gas flow rate. The presence of gas bubbles has two effects on the transition velocity. On one hand, gas bubbles tend to lower the viscosity and density of the pseudo-carrying fluid, where gas and liquid phases are considered as one phase. This characteristic reduces the carrying capacity of fluidizing media. On the other hand, the wake of gas bubbles enhances the upward motion of solid particles, leading to an increased carrying capacity. Large bubbles always occur at high gas flow rates. At a low gas flow rate (less than 66 mL/s), the decrease in fluid viscosity and density dominates. Hence, the liquid velocity required for the transition from the expanded bed to the circulating regime appears to increase. The bubble wake effect became more important when gas flow rate is high enough, which results in a lower transition liquid velocity. The same phenomenon was not observed in the system of 433-μm glass beads. These particles have a lower particle terminal velocity, and are therefore easily carried upward. The gas flow only facilitates this motion.

Fig. 8 shows that the transition liquid velocity of the flow system reduced when the liquid viscosity was increased. An increase in the liquid viscosity enhanced the shear stress acting on the particles. This increase resulted in a higher drag force, and therefore, the circulation regime was reached at a lower transition velocity.

4.2.2. Comparison of the transition velocity determined by different methods

The transition velocities determined using the discriminant analysis approach were compared to the ones obtained

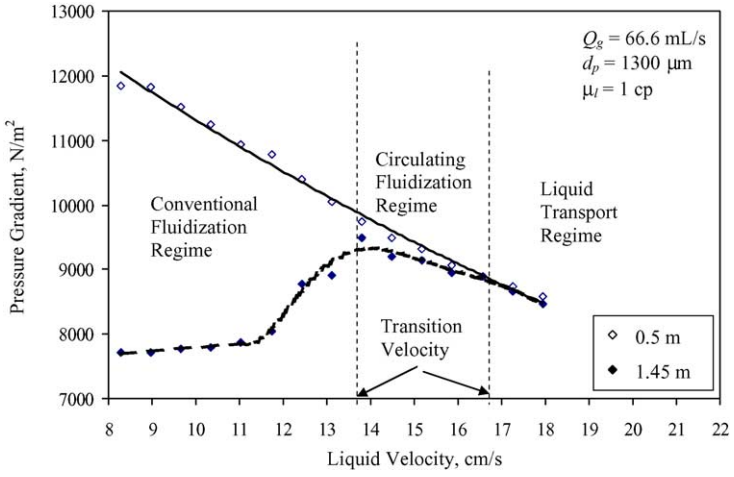

Fig. 9. The pressure gradient variation measured at two elevation in a three-phase fluidized bed at gas flow rate of 66.6 mL/s, using 1300-μm glass beads and 1-cP water.

by the pressure gradient variation and the solid circulating rate methods.

The pressure gradient variation method was first presented by Liang et al. [2]. The pressure gradients at two axial locations were plotted as a function of total liquid velocity. For an example, Fig. 9 shows the results obtained in the 1300-μm glass bead system with a fixed gas velocity of 66.6 mL/s. The pressure gradient at the lower test section (0.5 m) kept decreasing with increasing liquid velocity. This characteristic was created by the expansion of the bed. On the other hand, the pressure drop measured at the upper test section (1.45 m) was started to increase with increasing liquid velocity at a liquid flow of about 11.4 cm/s. When the value of the liquid velocity was 13.6 cm/s, the pressure gradient reached a maximum value. At this point, the transition between the expanded and circulating fluidization regimes was defined. With further increase in the liquid velocity, the pressure gradient started to drop quickly. At a liquid velocity of approximately 16.6 cm/s, the pressure gradients at the two measurement locations were merged into one curve. There was no variation of the pressure drop in the fluidization unit, and the critical boundary between the circulating and the transport fluidization regimes was obtained.

Under the same operating conditions, the result obtained using the solid circulating rate method is presented in Fig. 10. This method, firstly proposed by Liang et al. [10], shows the relationship between the solid circulating rate and the liquid velocity. At a liquid velocity of about 13.4 cm/s, the solid circulating rate in the system started to increase from the zero to non-zero value. At this point, the system entered the circulating fluidization regime. With further increasing liquid velocity till the liquid velocity was at about 16 cm/s, the liquid velocity finally had no influence on the solid circulating rate, and the fluidization transferred from the circulation fluidization regime to the transport one.

The transition liquid velocities obtained using the pressure profile method and the solid circulating rate method are listed in Table 1. In addition, Table 1 also presents the transi-

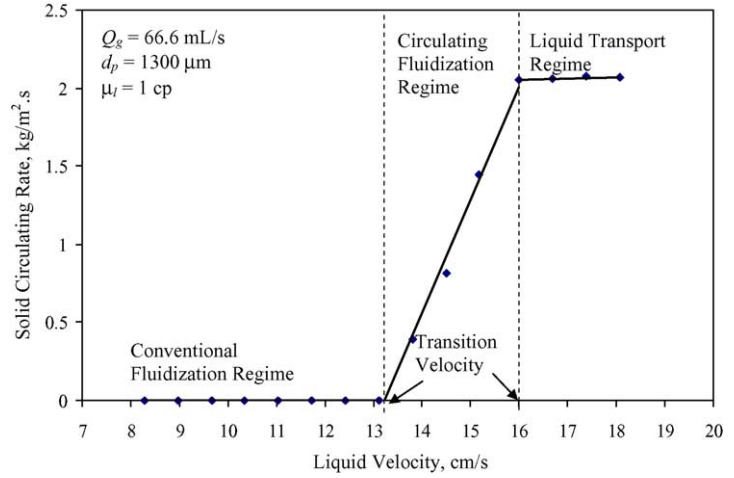

Fig. 10. Relationship between solid circulating rate and liquid velocity in a three-phase fluidized bed at gas flow rate of 66.6 mL/s, using 1300-μm glass beads and 1-cP water.

Table 1
Comparison of the regime transitions in the three-phase fluidized bed obtained by the pressure profile and the solid circulating rate methods

d_p (μm)	μ_l (cP)	Q_g (mL/s)	Transition velocity between expanded and circulating regimes (cm/s)		Transition velocity between circulating and transport regimes (cm/s)	
			ΔP method[a]	G_s method[b]	ΔP method[a]	G_s method[b]
700	1	0	6.4	7	10.7	10
		35.1	8	7.4	11.7	12.1
		66.6	8.9	8.9	11.4	11.3
		113.6	7.6	8.1	–	12.6
1300	1	0	12.6	12.8	15.4	15.5
		35.1	12.7	12.9	15.2	15.3
		66.6	13.6	13.4	16.6	16
		113.6	13.3	12.6	–	16.3

[a] Pressure gradient profile method.
[b] Solid circulating rate method.

tion velocity between the circulating and transport fluidization regimes obtained by the pressure profile and the solid circulating rate methods. The results of these two methods agreed well to each other.

Fig. 7 compares the transition velocities between the expanded and circulating fluidization regimes determined by the new mathematical approach, with the two previously reported; the pressure profile method and the solid circulating rate method. A good agreement was obtained. Moreover, Liang et al. [2] reported that the transition velocity of the circulating fluidization was about 6.1 cm/s for a three-phase fluidized bed using 405-μm glass beads with a gas flow rate of 82.09 mL/s. This result was also in good agreement with the transition velocity calculated by the discriminant analysis for a similar fluidization system, as shown in Fig. 7. Therefore, it can be concluded that the discriminant approach is reliable and effective for the prediction of the boundary between expanded bed and circulating fluidization regime under the wide range of operating conditions.

4.2.3. Comprehensive approach

The aforementioned approach requires a complete discriminant analysis to be performed for each experimental condition, as the physical property of fluidizing media and the particle size are not taken into account. Thus, to include these factors, a comprehensive study is proposed here. A comprehensive liquid velocity is defined as one discriminant variable to consider the effect of gas flow rate, liquid viscosity, and particle size. The other variable was the modified standard deviation, which can be expressed as,

$$\frac{\sigma U_l \mu_l}{d_p U_g} \tag{13}$$

where σ is the standard deviation of the conductivity signals. U_l is the liquid velocity, U_g the gas velocity, d_p the average particle size and μ_l the liquid viscosity. The analysis was performed on 65 sets of experimental data operating under the expanded three-phase fluidization system, and 50 sets of data taken under the conditions of circulating fluidization system. The comprehensive discriminant index was computed to be 0.054, which corresponded to the critical comprehensive liquid velocity of 8.9 cm/s (Fig. 11).

The significance of the separation between the two groups was tested using the F-test described earlier (Eqs. (11)–(12)). The calculated value was 84.58, which was much higher than the F-number at the standard level of 0.05 (equal to 3.08). This condition confirmed that the choice of these two variables was valid.

The comprehensive discriminant index, Y_{AB}, was then used to classify 35 sets of experimental data. If the computed Y value was greater than 0.054, the system was in a circulating fluidization regime. Otherwise, the system was in an expanded fluidization regime. The transition boundaries obtained from the comprehensive approach were in good agreement with results calculated using the discriminant approach as shown in Table 2. Slight discrepancy between these two methods was observed around the transition region. This dis-

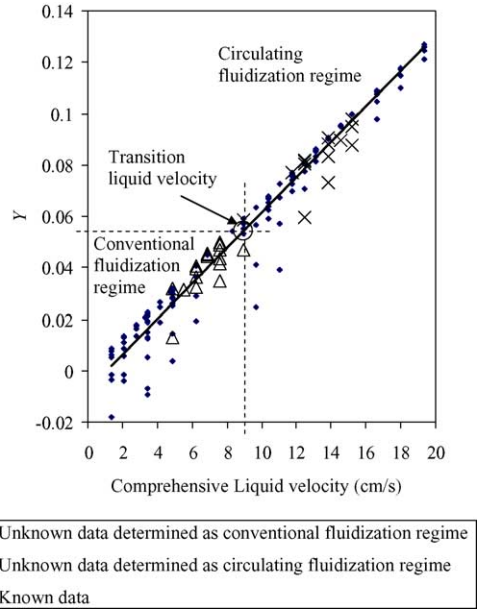

Fig. 11. The relationship between Y and liquid velocity for the comprehensive study of the discriminant analysis.

Table 2
Comparison of the results obtained by the two discriminant analysis approaches

d_p (μm)	μ_l (cP)	Q_g (mL/s)	U_l (cm/s)	Discriminant approach	Comprehensive approach
433	1	0	4.84	CON	CON
433	1	0	6.23	CON	CON
433	1	35.1	6.23	CON	CON
433	1	35.1	7.61	CON	CON
433	1	66.6	5.53	CON	CON
433	1	66.6	6.23	CON	CON
433	1	66.6	7.61	CFB	CON
433	1	113.6	4.846	CON	CON
700	1	0	7.61	CON	CON
700	1	35.1	7.61	CON	CON
700	1	66.6	7.61	CON	CON
700	1	113.6	7.61	CON	CON
700	1	113.6	8.99	CFB	CON
433	1.8	15.1	7.61	CON	CON
433	1.8	15.1	6.92	CON	CON
433	1.8	35.1	6.92	CON	CON
433	1.8	55	6.92	CON	CON
433	1	66.6	8.99	CFB	CFB
433	1	35.1	8.99	CFB	CFB
1300	1	0	12.45	CON	CFB
1300	1	0	13.84	CFB	CFB
1300	1	35.1	13.84	CFB	CFB
1300	1	35.1	15.22	CFB	CFB
1300	1	66.6	13.84	CFB	CFB
1300	1	66.6	14.53	CFB	CFB
1300	1	66.6	15.22	CFB	CFB
1300	1	113.6	12.45	CON	CFB
1300	1	113.6	13.84	CFB	CFB
1300	1	113.6	15.22	CFB	CFB
433	1.8	35.1	12.45	CFB	CFB
433	1.8	55	12.45	CFB	CFB

CON—gas–liquid–solid expanded fluidized bed. CFB—gas–liquid–solid circulating fluidized bed.

crepancy may have been caused by the lower precision of the comprehensive method due to the combination of a number of operating factors. However, the comprehensive discriminant analysis proved to be another reliable approach. The comprehensive analysis has good potential for on-line monitoring of the fluidization status in industrial applications since conductivity detection is a common practice.

5. Conclusions

The fluctuations of the conductivity voltage signals within the three-phase fluidized bed are affected by liquid viscosity, particle size and operating conditions, such as gas flow rate and liquid velocities. The nature of the voltage signal fluctuation led to the new successful approach, which is based on the discriminant analysis, to define the boundary between the expanded and the circulating fluidization regimes. The results from this new approach, using the liquid velocity and the standard deviation of conductivity voltage as discriminant variables, are in good agreement with the values of the pressure gradient and the solid circulating rate methods. Moreover, the comprehensive approach combining the effects of liquid viscosity, particle size and gas and liquid velocities is proved to be a reliable approach to define the transition velocity between these two regimes as well. The transition liquid velocity is a function of the operating conditions and the physical properties of liquid and solid phases.

Acknowledgments

The authors gratefully acknowledge the financial assistance from NSERC and Chemical Engineering Department, University of New Brunswick. Help provided by Jonathan Procopio is highly appreciated.

References

[1] L.-S. Fan, R.H. Jean, K. Kitano, On the operation regimes of cocurrent upward gas-liquid-solid systems with liquid as the continuous phase, Chem. Eng. Sci. 42 (1987) 1853–1855.
[2] W.G. Liang, Q.W. Wu, Z.Q. Yu, Y. Jin, H.T. Bi, Flow regimes of the three-phase circulating fluidized bed, AIChE J. 41 (1995) 267–271.
[3] D. Kunii, O. Levenspiel, Fluidization Engineering, John Wiley and Sons, New York, 1977.
[4] J.M. Ham, S. Thomas, E. Guazzelli, G.M. Homsy, M.-C. Anselmet, An experimental study of the stability of liquid-fluidized beds, Int. J. Multiphase Flow 16 (1990) 171–185.

[5] J.M. Begovich, J.S. Watson, Hydrodynamic characteristics of three-phase fluidized beds, in: J.F. Davidson, D.L. Keairns (Eds.), Fluidization, Proceeding of the Second Engineering Foundation Conference, Cambridge University Press, UK, 1978, pp. 190–195.
[6] S.L.P. Lee, H.I. de Lasa, Phase holdups in three-phase fluidized beds, AIChE J. 33 (8) (1987) 1359–1370.
[7] F. Larachi, M. Cassanello, M. Marie, J. Chaouki, C. Guy, Solid circulation patterns in three-phase fluidized bed containing binary mixtures of particles as inferred from RPT, Trans. IchemE 73 (A) (1995) 263–268.
[8] D.L. George, K.A. Shollenberger, J.R. Torczynski, T.J. O'Hern, S.L. Ceccio, Three-phase material distribution measurements in a vertical flow using gamma-densitometry tomography and electrical-impedance tomography, Int. J. Multiphase Flow 27 (2001) 1903–1930.
[9] J.-M. Schweitzer, J. Bayle, T. Gauthier, Local gas hold-up measurements in fluidized bed and slurry bubble column, Chem. Eng. Sci. 56 (2001) 1103–1110.
[10] W. Liang, Q. Wu, Z. Yu, Y. Jin, Z. Wang, Hydrodynamics of a gas-liquid-solid three-phase circulating fluidized bed, Can. J. Chem. Eng. 73 (1995) 656–661.
[11] L.-S. Fan, Gas–Liquid–Solid Fluidization Engineering, Butterworths Publishers, MA, 1989.
[12] J.-P. Zhang, J.R. Grace, N. Epstein, K.S. Lim, Flow regime identification in gas–liquid flow and three-phase fluidized beds, Chem. Eng. Sci. 52 (1997) 3979–3992.
[13] Y. Jin, J.-X. Zhu, Z.-Q. Yu, Novel configurations and variants, in: J.R. Grace, A.A. Avidan, T.M. Knowlton (Eds.), Circulating Fluidized Bed, Blackie Academic and Professional, London, UK, 1997, pp. 525–567 (Chapter 16).
[14] W.R. Klecka, Discriminant Analysis, Sage, USA, 1980.
[15] J.C. Davis, Statistics and Data Analysis in Geology, second ed., J. Wiley, USA, 1973, pp. 442–473.
[16] T. Cacoullos, Discriminant Analysis and Applications, Academic Press, USA, 1973.
[17] H.W. Kwon, Y.K. Kang, S.D. Kim, M. Yashima, L.T. Fan, Bubble-chord length and pressure fluctuations in three-phase fluidized beds, Ind. Eng. Chem. Res. 33 (1994) 1852–1857.
[18] W. Luewisutthichat, A. Tsutsumi, K. Yoshida, Chaotic hydrodynamics of continuous single-bubble flow systems, Chem. Eng. Sci. 52 (1997) 3685–3691.